The most prevalent Freeman-Sheldon Syndrome mutations in the embryonic myosin motor share functional defects

Jonathan Walklate[1], Carlos Vera[2], Marieke J. Bloemink[1,3], Michael A. Geeves[1]* and Leslie Leinwand[2]*

[1]School of Biosciences, University of Kent, Canterbury, CT2 7NJ, UK
[2]Department of Molecular and Developmental Biology, University of Colorado, Boulder, Colorado 80309, USA
[3]Present address: M.J. Bloemink, Biomolecular Research Group, School of Human and Life Sciences, Canterbury Christ Church University, Canterbury, United Kingdom.

*Joint corresponding authors

Running Title: Freeman-Sheldon Syndrome mutations in human embryonic myosin

Address Correspondence to:
Michael A. Geeves, School of Biosciences, University of Kent, CT2 7NJ, UK;
Tel +44 1227 827597; E-mail: M.A.Geeves@kent.ac.uk

Leslie Leinwand, Department of Molecular and Developmental Biology, University of Colorado, Boulder, Colorado 80309, USA;
Tel +1 303 4927606; E-mail: leslie.leinwand@Colorado.EDU

Key words
enzyme kinetics, molecular motor, recombinant protein expression, skeletal muscle, ATPase
myosin subfragment 1, stopped-flow, human myosin, transient kinetics, motor domain, muscle disease

Abstract

The embryonic myosin isoform is expressed during fetal development and rapidly down-regulated after birth. Freeman-Sheldon Syndrome (FSS) is a disease associated with missense mutations in the motor domain of this myosin. It is the most severe form of distal arthrogryposis leading to over contraction of the hands, feet, and orofacial muscles, and other joints of the body. Availability of human embryonic muscle tissue has been a limiting factor in investigating the properties of this isoform and its mutations. Using a recombinant expression system we have studied homogeneous samples of human motors for the wild type (WT), and three of the most common FSS mutants: R672H, R672C, and T178I. Our data suggest that the WT embryonic myosin motor is similar in contractile speed to the slow type I/β cardiac based on the rate constant for ADP release and ADP affinity for actin.myosin. All three FSS mutations show dramatic changes in kinetic properties, most notably, the slowing of the apparent ATP hydrolysis step (reduced 5-9 fold) leading to a longer lived detached state and a slowed V_{max} of the ATPase (2-35 fold), indicating a slower cycling time. These mutations therefore seriously disrupt myosin function.

Introduction

Autosomal dominant mutations in 5 of the 10 human sarcomeric myosin heavy chain (MyHC) genes cause a wide variety of cardiac and skeletal myopathies (1); and new mutations continue to be discovered (2-5). There are 2 developmental myosin isoforms: MyHC-perinatal (MYH8) and MyHC-embryonic (MYH3) both of which are expressed primarily during fetal development and during muscle regeneration (6).

There have been few studies of developing muscle in humans, however, the order in which myosin isoforms are expressed has been described. Primary skeletal muscle fibers appear after 8 weeks of gestation followed at 10 weeks by the appearance of secondary fibers which become the predominant form by week 21 (7). Primary fibers express MyHC-emb and the cardiac or slow muscle isoform, MyHC-β (8, 9), with the MyHC-emb being detected before MyHC-β (10). Secondary fibres initially only express MyHC-emb followed by MyHC-peri (10). At week 15 MyHC-emb accounts for about 81 % of all human MyHC transcripts (11), while a population of tertiary fibers emerges at week 16

that expresses adult fast myosin (9, 12). Adult myosins and tertiary fibres gradually increase towards the end of gestation (9, 10) as both MyHC-emb and MyHC-peri are downregulated with MyHC-emb and MyHC-peri only being faintly detectable in a few fibers in 1 month old infants. However, recently MyHC-emb protein has been detected outside this time window (13).

Mutations in MyHC-emb cause autosomal dominant distal arthrogryposis (DA2A), the most severe form of which is Freeman-Sheldon Syndrome (FSS) (11). Phenotypes include club foot, camptodactyly (contractures of the fingers or toes), contractures of oral facial muscles leading to a 'whistling face' phenotype, and in the most severe cases, scoliosis (14). There are currently 8 identified MyHC mutations that cause FSS (14-16). 90% of FSS cases are linked to 3 mutations in the motor domain of MyHC-emb: R672C, R672H and T178I (14). Patients who have the T178I mutation have the most severe phenotypes (facial contractures and congenital scoliosis), R672H results in intermediate severity and R672C is the least severe (14). Adult muscle fibres from individuals with wild type MyHC-emb and those with the R672C mutation do not differ in expression levels of MyHC-emb protein (13). Tajsharghi et al (2008) (17) presented data from a FSS patient with a T178M mutation in MYH3. At 15 months the individual had a higher level of MyHC-peri expression (>20% of all fibers) compared to that of 8 'healthy' control samples (0 – 2% of all fibers) taken at a similar time of development (10-15 months). Samples taken from the same patient at 5 years showed a predominance of type-1/MyHC-β expression with small, scattered type-1 fibers. This suggests that there could be a compensatory effect or a developmental defect which causes MyHC-peri to be expressed later or longer in postnatal development. Tajsharghi et al (2008) hypothesised that the myopathy occurs during embryonic development and that after birth, when MyHC-emb is downregulated, there is a recovery of the muscle leaving some residual muscle defects. Functional studies on muscle fibers from healthy and FSS individuals with the R672C mutation showed that the mutant fibers had reduced force, prolonged relaxation time, and incomplete relaxation (13).

Embryonic myosin heavy chain is the most abundant during development when muscles are being formed (6). Since distal muscles are more affected in FSS, it is interesting to note that distal muscles appear to be formed earlier during development than proximal muscles (18). They may therefore express embryonic myosin for a longer period of time than proximal muscles.

To understand the pathogenesis of FSS, it is necessary to understand the nature of the defect in the mutant myosin motor proteins and how it might be corrected. Both residues involved, T178 and R672, are highly conserved in all myosin II molecules and located near the ATP binding site close to the P-loop where the γ-phosphate of ATP binds (Figure 1). Examination of homologous myosin motor domain structures (subfragment 1 or S1; Figure 1a) shows that T178 is at the end of 4th strand of the central 7 stranded β-sheet and close to the ATP binding site at the base of the P-loop (Figure 1b) in a location that can influence ATP binding and hydrolysis. R672 is located on the 3rd β-strand with the side chain buried and which interacts with the relay helix, SH1-SH2 domain and the β-strands on either side, regions which go through major conformational changes during the myosin cross-bridge cycle (19, 20). Notably the crystal structures show an interaction between R672 and T178 which may account for the similar phenotypes in the mutants.

Due to the difficulty of isolating homogeneous myosin samples from human muscle and the limited ability to obtain samples from FSS patients, we utilised an established recombinant expression approach (21). This approach was first used by Wang et al. (22) and we have used it to study the kinetics of all human adult skeletal and cardiac isoforms, and two mutations in the human cardiac MyHC-β associated with hypertrophic cardiomyopathy (HCM) (23-25). These studies have demonstrated that this is a powerful technique for studying homogeneous, human, wild type and mutant myosin S1 samples using both biochemical kinetics and in vitro motility approaches. We used this recombinant approach to study pure human WT MyHC-emb and the 3 FSS-causing mutants. Although some results have been reported on embryonic and R672C mutant muscle fibres (11); (13), to our knowledge this is the first detailed functional study of purified WT MyHC-emb and any of the mutations that cause FSS.

Methods

Proteins – Human embryonic MyHC-S1 proteins were expressed and purified as described previously Resnicow et al. 2010 (21). We constructed shuttle plasmids containing the S1 coding region for MYH3 (Met1-Ser843) upstream of a 6x-Histidine tag. Using the

pAdEasy kit these plasmids were used to construct recombinant replication-deficient adenovirus that express MYH3. We first cloned the WT MYH3 gene and then performed site-directed mutagenesis to produce the R672C, R672H and T178I mutations. The viral particles were amplified using HEK293 cells and the cell lysates were clarified using cesium chloride gradients and the concentrated virus was stored in a glycerol buffer at –20 °C.

Infected C_2C_{12} cells were incubated for 5 days and frozen into a cell pellet. This was then homogenized in a low salt buffer, centrifuged and the supernatants purified by two procedures. For stopped-flow we used nickel affinity chromatography (HisTrap HP 1 ml column). Afterwards the S1 was dialysed into the low salt stopped-flow buffer (25 mM KCl, 20 mM MOPS, 5 mM $MgCl_2$, 1 mM DTT, pH 7.0, Figure 2). From between 1500-3000 cm^3 of cultured C_2C_{12} cells we isolated 1-2 mg of purified MyHC with a concentration between 10-20 µM. A small amount of endogenous myosin persisted in the S1 sample purified for stopped-flow. Using densitometry software (Scion Image) to analyse SDS-PAGE gels we calculated the contaminate myosin as < 5% of the S1 by mass; or 1:40 molar ratio of myosin: S1. It is possible that the myosin and S1 were bound to actin and so were co-purified.

For ATPase measurements the purification scheme was modified and extended. Nickel affinity chromatography was performed by gravity in Bio-Rad Econo-Pac column packed with HisPur Ni-NTA Resin. Eluates were dialyzed in a low-salt/low-imidazole buffer. The eluted material was subjected to anionic exchange chromatography (HiTrap HP 1 mL column) and desalted by another buffer exchange into the ATPase assay buffer (see ATPase method). This gave a higher purity of S1 necessary for ATPase assays.

As previously reported (21) the recombinant S1 co-purifies with the endogenous mouse light chains (Figure 2). Essential light chains (ELC) MLC1A, MLC1F and regulatory light chain (RLC) MLC2F appear to purify with the recombinant S1 since their bands are much denser than the ELC MLC3F and in the correct ratio to the heavy chain. They are the same light chains that have been found to associate with embryonic myosin in tissue (26). The percentage identity between the human and mouse light chains are 90-95%. Rabbit skeletal actin was prepared as previously described (Pardee & Spudich 1982) and labelled with pyrene at Cys-374 (Criddle 1985).

ATPase - For steady-state ATPase measurements we modified the NADH-coupled assay as described in (27). This assay system couples the ADP production to NADH oxidation to NAD^+, therefore absorbance was read at 340 nm. We used a 96-well format and the assay buffer used in all experiments was 12 mM PIPES, 2 mM $MgCl_2$, and 1 mM DTT at pH 6.8 and 25 ºC. Bovine cardiac actin was purified as previously described (Pardee & Spudich) and used for ATPase measurements. Once thoroughly and rapidly mixed the assays was read for 30 min in a Molecular Devices SpectraMax to monitor absorbance over time. The Michaelis-Menten equation was fit to the data to determine the maximal activity (V_{max}) and the associated actin constant for myosin (K_M) using GraphPad Prism.

Transient kinetics – All kinetic experiments were conducted in 20 mM MOPS buffer with 25 mM KCl, 5 mM $MgCl_2$, and 1 mM DTT , pH 7 at 20 °C, unless otherwise indicated. Measurements were performed with a High-Tech Scientific SF-61 DX2 stopped-flow system. The concentrations stated are those after mixing in the stopped-flow observation cell unless otherwise stated. All stopped-flow traces were analysed in either software provided by TgK Scientific (Kinetic Studios) or Origin (Microcal). Intrinsic tryptophan fluorescence was measured by excitation at 295 nm and observed through a WG320 filter. In the absence of actin the kinetics of S1 and ATP or ADP were interpreted using the seven-step model described by Bagshaw et al. (28) (Scheme 1), where the forward rate constants are k_{+i} and the reverse rate constants are denoted k_{-i}. $K_i = k_{+i}/k_{-I}$ representing the equilibrium constant at the ith step in the reaction.

In the ADP displacement from S1 assays the two amplitudes are proportional to the concentration of S1 present as either free S1 or S1.ADP. ADP concentrations determine the amplitudes as follows:

$$A_{slow} = \frac{A_{max}[ADP]}{K_5+[ADP]} + A_{min} \qquad \text{(Eq. 1)}$$

$$A_{fast} = \frac{A_{max}K_5}{[ADP]+K_5} + A_{min} \qquad \text{(Eq. 2)}$$

When actin was present, the sample was excited at 365 nm, emission of pyrene-labelled actin was detected after being passed through a KV399 cut-off filter. The binding of S1 to pyrene-labelled actin quenches the fluorescence therefore dissociation could be measured by an increase in fluorescence. The interactions between acto.S1

and ATP or ADP were analysed based on the model in scheme 2 (23)

Following a reversible binding of ATP to actomyosin there is a rate-limiting isomerisation (k'_{+2}) of the complex leading to rapid actomyosin dissociation. ADP and ATP compete for the nucleotide binding site on the S1 and ADP binding is governed by the dissociation constant K'_5 ($=k'_{+5}/k'_{-5}$).

A dissociation reaction can be measured when the pyrene-labelled actin is in a complex with S1 since the complex quenches the pyrene signal. ATP induces the dissociation of S1 from actin resulting in an increase in fluorescence allowing the reaction kinetics to be determined. Using scheme 2, Eq. 3 can be used to determine the constants $K'_1k'_{+2}$, k'_{+2}, and $1/K'_1$.

$$k_{obs}=\frac{K'_1k'_{+2}[ATP]}{1+K'_1[ATP]} \qquad \text{(Eq. 3)}$$

Eq. 4 defines the kinetics when ATP and ADP are in rapid competition for binding to the actomyosin complex and that $K'_1[ATP] < 1$, such that the equation is linear with respect to [ATP].

$$k_{obs}=\frac{K'_1k'_{+2}[ATP]}{1+\frac{[ADP]}{K'_5}} \qquad \text{(Eq. 4)}$$

If in the absence of ADP the $k_{obs} = k_0$ then normalizing Eq. 4 can make different myosin isoform comparisons easier.

$$k_{rel}=\frac{k_{obs}}{k_0}=\frac{1}{1+\frac{[ADP]}{K'_5}} \qquad \text{(Eq. 5)}$$

To determine the actin affinity a S1 titration assay was performed as described by Kurzawa and Geeves (29). Fixing the concentration of pyrene-labelled actin the amplitude of the ATP induced dissociating reaction provides an estimate of the fraction of actin bound to S1 at increasing S1 concentrations. The amplitude dependence of S1 concentration was fitted to the physically significant root of the following quadratic equation.

$$\alpha=\frac{[M]+K_D+[A]_0-\sqrt{([M]+K_D+[A]_0)^2-\frac{4}{[M][A]_0}}}{2[A]_0} \qquad \text{(Eq. 6)}$$

In all cases, the data in the figures refer to individual experimental measurements, whereas Table 1 gives mean values of the fitted constant for a minimum of three separate measurements using different protein preparations.

Sequence Alignments and Homology Modelling – Three-dimensional homology models were generated (Figure 1) for the human embryonic isoform using SWISS-MODEL automatic comparative protein modelling server (30-33). The primary sequence for the embryonic myosin was pairwise aligned with the sequence of the six scallop structures (PDB codes given below) using CLUSTAL OMEGA alignment protocol. These alignments were submitted to SWISS-MODEL which generated the models. The sequence identity between the human embryonic S1 sequence and the scallop myosin was 60% so allowed us to build well resolved structures. The scallop structures were used because they represent different conformational states of the cross-bridge cycle: post-rigor like structure with ADP bound (PDB code 2OTG), a rigor like structure without nucleotide bound (PDB code 2OS8), a post rigor structure without a nucleotide bound (PDB code 1SR6), a pre-power stroke state containing ADP-VO_4 (PDB code 1QVI), the actin-detached state containing ADP-BeF_x (PDB code 1KK8), and a near rigor state with ADP bound (PDB code 1S5G). We compared the interactions we found in the homology to the two MyHC-β structures (4P7H and 4DB1, sequence identity 79%) to validate their existence in human myosin structures as well as the original scallop structures.

Results

Nucleotide binding to actin.S1 and actin binding to S1

The detachment of the actin.myosin cross-bridge is the step that is thought to limit shortening velocity in contracting muscle fibers. This can be limited by either the rate of ATP binding to the cross-bridge or the preceding ADP release step (Scheme 2). Since these are the first reports of detailed kinetics of wild type (WT) MyHC-emb, we will compare its properties to another slow myosin, the well-characterized MyHC-β. For slow type myosins the affinity of ADP for actin.S1 is normally tighter than the fast type myosins (IIa, IIb, IIx, α) and ADP release limits the detachment and the overall muscle shortening velocity (34-36). Therefore we examined these steps first.

ATP induced detachment from actin is slower for myosin S1 carrying FSS mutations – The ATP induced dissociation of S1 from actin was monitored by the fluorescence of a pyrene label covalently attached to Cys-374 of actin (Figure 3A). At low concentrations of ATP WT MyHC-emb, R672C and T178I are best described by a single exponential fit. At all ATP concentrations there is a second slower phase for R672H, which is best described by a double exponential fit. At high ATP concentrations ([ATP] > 100 μM) T178I develops a slow second

phase, similar to the slow component in R672H. A slow component was not seen for the WT MyHC-emb or the R672C at any concentration of ATP used. At low ATP concentrations there is a linear relationship between k_{obs} and ATP concentration for all constructs (Figure 3B) which gives a second order rate constant of actin dissociation ($K'_1k'_{+2}$, Table 1). Compared to β-cardiac myosin S1, the WT MyHC-emb shows faster ATP-induced dissociation kinetics whereas for the FSS mutants this process is slower (Table 1, see Figure 9).

The maximum rate of ATP induced dissociation is significantly altered by the FSS mutations – Over larger ATP concentrations, the relationship between k_{obs} and ATP concentration is best described by a hyperbola (Figure 3B) which gives a maximum rate constant of dissociation (k'_{+2}) and the affinity of ATP binding in the initial step $1/K_1$. There is a second slow component found at all ATP concentrations for R672H and at the higher ATP concentration (>100 μM) for T178I. One cause of a slow component could be ADP contamination, therefore S1 was incubated with apyrase to hydrolyse any ADP; however this has no effect on the slow component for either the R672H or T178I. This led us to the hypothesis that the slow component is caused by a conformational change in the ATP binding pocket from a closed to open state (K_α, Scheme 2) previously seen in MyHC-β (37) (Table 1). The maximum rate constant of opening from the closed conformation ($k_{+\alpha}$) is summarised in Table 1. Using the ratios of the fluorescence amplitudes for both components it is possible to calculate the equilibrium constant of the conformational change (K_α, Table 1).

***ADP affinity (K'*$_5$) for WT MyHC-emb motor domain and the 3 mutations is typical of a slow myosin** – To determine ADP affinity in the presence of actin, a competition assay was used (Figure 4A). The observed rate constant (k_{obs}) reduces as ADP increases and exhibits a hyperbolic dependence on ADP concentration defining the ADP-affinity, K'_5 (Figure 4B). A similar measurement for T178I results in a value of K'_5 which is not significantly different from that for WT MyHC-emb. The ADP affinity for WT MyHC-emb is about 2-fold weaker than the WT β-myosin S1. The FSS mutation T178I does not alter ADP affinity compared to WT MyHC-emb.

The hyperbolic dependence of k_{obs} on ADP concentration, found for WT MyHC-emb and T178I, is consistent with the rate constant of ADP release being of the same order or faster than the rate constant for ATP binding (K_1k_{+2}[ATP]) under these conditions. This was confirmed by measuring the rate of ADP displacement directly by incubating the actin-S1 complexwith a much higher ADP concentration and displacing with several high ATP concentrations (see Figure 5) (37).

This type of hyperbolic dependence on ADP concentration is not found for the other two mutations (R672H and R672C) which shows a biphasic transient (Figure 4C). This is consistent with the rate constant for ADP release (k'_{+5}) being slower than the rate constant for ATP binding. The fast phase results from ATP binding to the fraction of actin.S1 which is free of ADP while the slow phase arises from the fraction of myosin as actin.S1.ADP from which ADP must first dissociate before ATP can bind.

For R672H the observed rate constant of the slower phase remains constant while the amplitude increases at increasing ADP concentration. In contrast, the fast phase amplitude decreases while the observed rate constant also remains constant (Figure 4C). A similar behaviour was also seen for the R672C mutation. When the fast and slow phase amplitudes are plotted against ADP concentration, both could be described by a hyperbolic function (Figure 4D), giving an overall ADP affinity (K'_5). Comparing these three FSS mutants to WT MyHC-emb, the ADP-affinity of R672H is about 3-fold tighter whereas for R672C and T178I this parameter is not significantly affected (Table 1).

FSS mutations reduce the affinity of actin for myosin S1 but increase actin affinity in the presence of ADP – By preincubating 30 nM pyrene-labelled actin (concentration before mixing) with varied S1 concentrations and then rapidly mixing with 20 μM ATP (concentration before mixing, Figure 5A) it is possible to determine actin affinity (K_A, Figure 5B). This measurement was repeated for the three FSS mutations. R672C and T178I have a similar K_A value as WT MyHC-emb, while R672H has an affinity almost 20-fold weaker compared to WT MyHC-emb (Table 1).

This assay was repeated with a constant saturating ADP concentration (20x the K'_5 value) preincubated with the acto-S1 mixture to determine the actin affinity in the presence of ADP (K_{DA}). The affinity of the WT MyHC-emb for actin weakens 250-fold (Figure 5C). All the mutants however have an affinity 2-4 fold tighter

than the WT (Table 1). This measurement also gives an estimate of the ADP release rate constant (k'_{+5}) where a saturating ADP concentration is displaced by a high ATP concentration and is independent of ATP concentration. This results in a single exponential, the k_{obs} is therefore linked to the k_{+5} value. Neither R672C nor T178I have a significantly different ADP-release rate than WT MyHC-emb, whereas R672H has an almost 3-fold slower ADP-release rate. The ADP-release rate for WT MyHC-emb is significantly slower compared to cardiac β myosin (Table 1).

Nucleotide binding to myosin S1 in the absence of actin

In the absence of actin, ATP binding to myosin can be monitored by a change in the intrinsic tryptophan fluorescence. The fluorescence change is caused by structural changes induced by both ATP binding and the ATP hydrolysis step (Scheme 1 – steps 1-3). While the binding of ATP to myosin is not part of the working cross-bridge cycle, the hydrolysis step controls how long myosin remains detached from actin.

The FSS mutations reduce the ATP-binding and hydrolysis rates for MyHC-emb S1 – The binding and hydrolysis of ATP by myosin was observed via the intrinsic fluorescence of S1. S1 at 100 nM was mixed with varying concentrations of ATP (Figure 6A).

All three FSS mutants have significantly slower k_{obs} values and smaller amplitudes than WT MyHC-emb. , and increasing the S1 concentration does not increase the amplitude The second order rate constant of ATP-binding, K_1k_{+2}, was determined by varying the ATP concentration and plotting k_{obs} as a function of ATP (Figure 6B). ATP-binding for WT MyHC-emb is about 2-fold faster than for β-myosin S1 and all three mutants have significantly lower second order rate constants compared to WT MyHC-emb (Table 1). The three FSS mutations strongly reduce ATP-binding to myosin S1 compared to WT MyHC-emb.

The maximum rate of ATP binding for WT MyHC-emb (k_{max}) was also determined from the hyperbolic fits (Fig 5B & Table 1). The value of k_{max} can either be attributed to the maximum rate of ATP binding (k_{+2}) with switch 1 and switch 2 closing or the hydrolysis step ($k_{+3} + k_{-3}$), which will be addressed in the discussion.

ADP-affinity is very tight for WT MyHC-emb and R672C – The ADP affinity of myosin-S1 can be measured by preincubating S1 with varying concentrations of ADP and rapidly mixing with excess ATP to displace the ADP. A two phase reaction is expected, consisting of a fast and a slow element representing the ATP binding to free S1 and ADP being displaced, respectively (Figure 6C). Increasing the concentration of ADP does not alter the k_{obs} for the fast or slow phase but does affect the amplitudes (Figure 6D) as more of the S1 is occupied by ADP that has to be displaced (slow phase) before ATP can bind. The measurement was repeated for each of the FSS mutations. However, the low fluorescence amplitudes observed on binding ATP made these measurements very difficult. The assay was only successful for R672C, and even then it was only possible to observe the loss of the fast phase. Using equation 5, the ADP-affinity (K_5) could be determined, however is not significantly different from the WT MyHC-emb (Table1). ADP displacement could not be measured for R672H and T178I because the 2% amplitude observed on ATP binding is too small to measure. Attempts to measure ADP binding using fluorescent nucleotides Mant- and Coumarin- modified ATP or ADP also result in no apparent change in fluorescence for R672H and T178I.

The V_{max} and K_M values of the three FSS mutants are reduced – The ATPase activity of the WT MyHC-emb and the three FSS mutants was measured as described in the methods. Both the values of V_{max} and K_M are significantly greater for WT than those for the mutants (Figure 7A). T178I data was plotted on a log [actin] scale (Figure 7B) to highlight that there is activation along with the increase in actin concentration. However the K_M is so low and the V_{max} so slow that this appears as a linear fit in Figure 7A. The values of V_{max} and K_M are summarised in Table 1 along with the V_{max}/K_M.

Homology models of the WT MyHC-emb and mutant motor domains show disrupted interactions between the ATP binding pocket and relay helix in the mutant proteins – We examined the local structural interaction of the two mutated residues R672 and T178 using embryonic homology models based on both scallop myosin II crystal structures These two residues are highly conserved throughout the myosin family and conserved in embryonic, cardiac and scallop myosin.

The homology models of WT MyHC-emb shows that residue R672 is buried in the core of the myosin molecule, located on the β3 strand of the central sheet. R672 interacts with residues on the two β strands on either side (β2 and β4) and

also with a residue located on the relay helix (F490). We will focus on two key interactions here whereas a more detailed summary of interactions can be found in Table 2A & B.

One key interaction is the H-bond between R672 and residue T178. T178 is located on β4 at the base of the P-loop which is involved in ATP binding and hydrolysis. This R672-T178 interaction is found in all conformational states available for WT MyHC-emb, indicating this H-bond is preserved as the myosin molecule goes through the cross-bridge cycle. For both the T178I and R672C mutations this hydrogen bond is lost in all myosin homology models whereas for the R672H mutant this H-bond remains present in the majority of the structures.

Another key interaction is the π-cation bond between R672 and residue F490. F490 is located on the relay helix close to a bend in the helix which develops during the recovery stroke and recovers at some point during the power stroke. This interaction is present in all WT MyHC-emb homology models but found to be consistently lost in both R672H and R672C mutations throughout the cycle. From our modelling it is difficult to know if the loss of the hydrogen bond between the T178 and R672 in the T178I mutant results in disruption of the π-cation bond between R672 and F490.

R672, located on the central β-sheet, appears to facilitate interaction between the β4 strand and the relay helix. Note that T178 is at the end of the β4 strand and is immediately adjacent to the P-loop motif ^{179}GESGAG^{184}. This motif is one of three loops that bind to the γ-Pi of ATP. Loss of coupling of P-loop movements to the relay helix by mutation to either R672 or T178 is expected to cause major disruption of the cross-bridge cycle.

Discussion

WT MyHC-emb has properties of a slow type myosin but differs significantly from the classic slow type myosin, MyHC-*β* – To our knowledge this is the first complete kinetic analysis of the human embryonic myosin S1 isoform. Comparison of the kinetic properties of WT MyHC-emb to the slow WT MyHC-β, see Table 1 and Figure 9, shows that there are significant differences between the two.

The high affinity of ADP for actin.myosin (K'_5 = 14 μM) and the slow rate constant for ADP release from actin.myosin (k'_{+5} = 22 s^{-1}) are indicators of a slow type myosin (38). The slow ADP release would result in a relatively long lived A.M.D complex (lifetime $1/k'_{+5}$ = 45 ms versus 17 ms for MyHC-β under these conditions) that has high affinity for actin (K_{DA} = 0.53 μM) and therefore could hold tension against a load. The slow ADP release rate constant is likely to limit the maximum shortening velocity ($V_o = d/\tau$ = working stroke / attached life time) to 5-10 nm/45 msec = 0.1-0.2 μm/sec. At the same time the ATPase V_{max} is similar for the two WT isoforms (6.0 and 7.0 s^{-1}) resulting in a higher unloaded duty ratio for the emb myosin (duty ratio = V_{max}/k'_{+5} = 0.33) compared to the β myosin (0.10).

The second order rate constant for ATP binding to actin.S1 ($K'_1k'_{+2}$), is two-fold faster for MyHC-emb than for MyHC-β. This is due to ATP affinity for actin.S1 (K'_1) being almost 4-fold tighter (84 vs 327 μM) for emb-S1 while the maximum rate of actin dissociation (k'_{+2}, 780 vs 1500 s^{-1}) is half that of MyHC- β. This means that the detachment of actin is slower at saturating ATP but much less sensitive to the concentration of ATP available than the MyHC-β. This could be important as the MyHC-emb could maintain its activity in fluctuating ATP concentrations. .

The fluorescence change associated with ATP binding to MyHC-emb S1 in the absence of actin is twice that of β-cardiac S1. The maximum k_{obs} for this process at saturating ATP concentrations is also 30 % faster and close to that expected for a fast muscle myosin. This fluorescence change has normally been assigned to the steps controlling ATP hydrolysis and the recovery stroke ($k_{+3} + k_{-3}$). ADP binding gave less than half of the fluorescence change for ATP binding to MyHC-emb suggesting the signal does primarily result from the change in the local environment of the conserved tryptophan at the end of the relay helix that is known to report the recovery stroke and hydrolysis step (39, 40). ADP affinity in the absence of actin is almost 4 times tighter for MyHC-emb than MyHC-β. However, in the presence of actin, the reverse is true. ADP affinity is almost 2-fold weaker for MyHC-emb. This results in a large increase in the thermodynamic coupling constant for ADP (K'_5/K_5), which increases almost 10-fold from 11.5 for MyHC- β to 95 for MyHC-emb. Thus, actin is much more effective at displacing ADP for MyHC-emb than for MyHC-β.

In summary, our data are consistent with MyHC-emb myosin being a slow type motor with a high nucleotide affinity as recently described by Racca et al (11). Our data also show that ATP binding ($K'_1k'_{+2}$) is 2-fold faster than MyHC-β, which is suggestive of a fast type myosins (41). However, the ADP release rate (k'_{+5}) is almost 3

times slower than MyHC-β which is indicative of a slow type myosin. Therefore MyHC-emb properties sit between the fast and slow type myosins.

The three FSS mutations significantly slow the cross-bridge cycle speed and alter the balance of the cycle at various steps – The V_{max} for the ATPase cycle is reduced substantially (2 to 30 fold) for all three mutations with at least 10 fold increases in the apparent affinity of actin (K_m). The rate constant for ADP release (limiting cross-bridge detachment) is little changed for T178I and R672C but reduced to 1/3rd for the R672H mutant. This results in estimates of the duty ratio ($= k'_{+5}/V_{max}$) being reduced in each case from 0.3 for WT MyHC-emb to ~0.18 for the two R672 mutations and very low for T178I (0.008). The two R672 mutations myosins would be able to sustain a lower force than the WT MyHC-emb and T178I would be very ineffective as a force holding myosin – consistent with this mutation having the most severe phenotype (11).

The major differences between the WT MyHC-emb and the three mutations in the cross-bridge cycle are ATP induced dissociation of actin from actin.S1 ($K'_1k'_{+2}$), ATP binding to S1 (K_1k_{+2}) and ATP hydrolysis (k_{+2} or $k_{+3} + k_{-3}$) (see Table 1 and Figure 9). The results suggest that ATP binding is slower than for WT MyHC-emb for all three mutations, by a factor 2 – 5 for actin S1 ($K'_1k'_{+2}$) and by 5- to 30-fold for S1 alone (K_1k_{+2}). The slowed rate constant for ATP binding is unlikely to have any physiological affect because the ATP in the cell is maintained at > 1 mM and each construct would be expected to bind ATP within 1 msec. The maximum rate constant of actin dissociation is, however, reduced 2- to 3-fold for the two R672 mutations and this would result in a longer lived A.M complex (2-3 msec).

One of the most striking changes is the reduction of $k_{+3} + k_{-3}$ by 5-10 fold. If this represents the ATP hydrolysis step then this would be a significant slowing of the ATPase cycle leading to the myosin spending more time detached from actin in each ATPase cycle. This is highlighted in comparing the rate constant of the hydrolysis step ($k_{+3} + k_{-3}$) with the V_{max} of the ATPase. For WT MyHC-emb the hydrolysis rate constant is more than 20 times the value of V_{max} while it is reduced to 10 and 7 for fold for the two R672 mutations.

A second point of interest is actin affinity with and without ADP present. In the absence of ADP, the actin affinities (K_A) of the three mutants are significantly reduced compared to the WT MyHC-emb. However, since the experiments were conducted with 30 nM pyrene-labelled actin and the K_A values are less than 10 nM (except for R672H), we can only conclude that the affinities are very tight and may even be the same. We can, however, say that the affinity of R672H for actin is significantly reduced; almost 20-fold weaker. The affinity in the presence of ADP (K_{DA}), on the other hand is 1.5- to 4-fold tighter for all three mutants compared to the WT MyHC-emb. The only significant difference between the three mutants for ADP affinity in the presence of actin was the R672H where K_5 was 3-fold tighter.

From these data (Table 1) it is clear that all three of the mutations have significant kinetic differences compared to the WT MyHC-emb. The common difference between the three is the reduced apparent rate of ATP hydrolysis.

The interaction between R672 and the relay helix is lost for the FSS mutants– This investigation was limited by the lack of tryptophan fluorescence change on ADP binding in the three mutants. Homology models for each mutation suggest a possible explanation for this loss of fluorescence. R672 and F490 (on the relay helix) form a π-cation bond, which is lost with the two R672 mutations. R672H has the potential to form π-π bonds (42) but none were observed in the homology models. These π-cation interactions form between positive ions or protein residues and the π face of a benzene ring or other aromatic structure (43). These interactions can be as strong as or even stronger than salt bridges, so a complete loss of such a contact could have a large effect on the protein. During the ATPase cycle the C terminus of the relay helix bends away from the β-sheet, with the tryptophan immediately after the relay helix reporting a change in fluorescence as it moves. Homology models for the rigor-like conformation of myosin (PDB code 2OS8) and the pre-power stroke conformation (PDB code 1QVI) revealed that F490 is located just before the point in the relay helix where it bends as part of the power stroke/recovery stroke (Figure 8A). F490 is one of three phenylalanines (Figure 8b) that had previously been identified as part of a fulcrum on the relay helix in myosin S1 (44). This work also showed that F489 and F490 sandwich F670 forming the fulcrum which stays locked together through the whole transition. It is possible that the π-cation bond between R672 and F490 plays a structural role in holding the fulcrum together and maintaining contact with the β sheet in which R672 sits.

Complete loss of this interaction in both R672 mutations could disrupt the structure of the fulcrum making it less stable. This translates into the loss of amplitude in the tryptophan fluorescence signal. , which indicates the relay helix is not moving properly in the recovery stroke and a slowing of the hydrolysis step linked to the recovery stroke. This complements the findings that the specific force of the R672C was reduced (13) as the conformational changes in the ATP and actin binding domains are not efficiently relayed to the converter domain and neck region.

A second important interaction is the hydrogen bond between R672 and T178. In the two mutations, R672C and T178I, this hydrogen bond is completely lost and is partially lost in the R672H. Destabilisation of this region is the probable cause for the reduction in the k_{+2} or k_{+3} + k_{-3} step seen for all three mutations. Therefore this bond between R672 and T178 must have some structural importance bringing the residues required for hydrolysis into proximity with the ATP. The loss of this bond could account for the reduction in the ATP hydrolysis rate. The reduction in tryptophan fluorescence in the T178I mutant also suggests that the bond between R672 and T178 is having an indirect effect on the π-cation bond from R672 to the relay helix.

The FSS mutations slow down the dissociation rate and once detached spend longer not bound to actin, leading to a longer ATPase cycle time – Our data support the finding that a longer, slower rate of relaxation as seen for FSS mutants (?) could be explained by a reduced detachment event (13). There was a 2-5 fold reduction in the second order rate constant for detachment ($K'_1k'_{+2}$) for the three mutations. However the reduction in the ATP hydrolysis step we have seen is a novel observation for the three FSS mutations. It is most likely that the destabilising effect of the mutations on the P-loop are having a detrimental effect on ATP binding and ATP hydrolysis. Furthermore, the loss of interactions between the central β sheet and the relay helix may hamper conformational changes within the molecule leading to the actin dissociation step. Both would lead to a longer cycling time where the myosin is bound to actin for longer or delayed in hydrolysing ATP. This would leave the myosin mainly in the M.T or A.M.T state, increasing the ATPase cycle time.

As the major myosin isoform expressed in embryonic development the effects of the mutant alleles of embryonic myosin should manifest themselves during the formation of skeletal muscle and its earliest function. Just as with most myosin based myopathies, the vast majority of reported cases of FSS are heterozygous; the prediction being that homozygous individuals would be inviable. It is noteworthy that FSS, a form of distal arthrogryposis, affects muscles in the lower legs and forearms, which appear to develop early relative to proximal skeletal muscle in fetal development (18). The timing and abundant expression of the mutant isoform during this stage could explain the symptoms seen post-birth; at a time when the expression of embryonic myosin has decreased significantly. Consistent with the joint contracture phenotype, these FSS mutations display severely reduced rate constants for cross-bridge detachment and slower cycling times. Understanding how the mutant myosin influences muscle contraction at different levels of expression along with the WT MyHC-emb myosin, or an up regulation of other myosins, would be important to determine. We are currently developing models to allow the behavior of different myosin isoforms in a sarcomere to be predicted (45, 46).

Acknowledgements: We would like to thank Ariana Combs, Steve Langer, and Max Gamelspacher for their assistance with cloning and protein production; MyoKardia for providing bovine actin, and Samantha Lynn for production of pyrene-labelled rabbit actin. Funding provided by the NIH grant: GM29090 to LL and Welcome Trust grant: 085309 to MAG.

Conflict of interest: The authors declare that they have no conflicts of interest with the contents of this article

Author contributions: CV produced gene constructs, grew adenovirus, transfected cell lines to produce all cell pellets, carried out steady state ATPase assays. JW purified proteins from cell pellets provided by CV and performed all transient kinetic assays except the preliminary studies performed by MB. LL & MAG designed the study and supervised data collection. All authors contributed to the interpretation of data, writing and editing the manuscript.

References

1. Oldfors, A. (2007) Hereditary myosin myopathies. Neuromusclar Disorders. **17,** 355-367

2. Hamady, M., Buvoli, M., Leinwand, L.A., and Knight, R. (2010) **Estimate of the abundance of cardiomyopathic mutations in the β-myosin gene**. International Journal of Cardiology. **144,** 124-126

3. Clarke, N.F., Amburgey, K., Teener, J., Camelo-Piragua, S., Kesari, A., Punetha, J., Waddell, L.B., Davis, M., Laing, N.G., Monnier, N., North, K.N., Hoffman, E.P., and Dowling, J.J. (2013) **A novel mutation expands the genetic and clinical spectrum of MYH7-related myopathies**
 . Neuromusclar Disorders. **23,** 432-436

4. Lamont, P.J., Wallefeld, W., Hilton-Jones, D., Udd, B., Argov, Z., Barboi, A.C., Bonneman, C., Boycott, K.M., Bushby, K., Connolly, A.M., Davies, N., Beggs, A.H., Cox, G.F., Dastgir, J., DeChene, E.T., Gooding, R., Jungbluth, H., Muelas, N., Palmio, J., Penttila, S., Schmedding, E., Suominen, T., Straub, V., Staples, C., Van den Bergh, P. Y. K., Vilchez, J.J., Wagner, K.R., Wheeler, P.G., Wraige, E., and Laing, N.G. (2014) Novel mutations widen the phenotypic spectrum of slow skeletal/β-cadiac myosin (MYH7) distal myopathy. Human Mutation. **35,** 868-879

5. Yüceyar, N., Ayhan, Ö, Karasoy, H., and Tolun, A. (2015) HomozygousMYH7R1820W mutation results in recessive myosin storage myopathy: Scapuloperoneal and respiratory weakness with dilated cardiomyopathy. Neuromusclar Disorders. **25,** 340-344

6. Schiaffino, S., Rossi, A.C., Smerdu, V., Leinwand, L.A., and Reggiani, C. (2015) Developmental myosins: expression patterns and functional significance. Skeletal Muscle. **5,**

7. Fidzianska, A. (1980) Human ontogensis. I. Ultrastructural characteristics of developing human muscle. Journal of Neuropathology and experimental Neurology. **39,** 476-486

8. Barbet, J.P., Thornell, L.E., and Butler-Browne, G.S. (1991) Immunocytochemical characterisation of two generations of fibers during the development of the human quadiceps muscle. Mechanisms of development. **35,** 3-11

9. Draeger, A., Weeds, A.G., and Fitzsimons, R.B. (1987) Primary, secondary and tertiary myotubes in developing skeletal muscle: A new approach to the analysis of human myogenesis. Journal of the Neurological Sciences. **81,** 19-43

10. Cho, M., Webster, S.G., and Blau, H.M. (1993) Evidence for myoblast-extrinsic regulation of slow myosin heavy chain expression during muscle fiber formation in embryonic development. The Journal of Cell Biology. **121,** 795-810

11. Racca, A.W., Beck, A.E., Rao, V.S., Flint, G.V., Lundy, S.D., Born, D.E., Bamshad, M., and Regnier, M. (2013) Contractility of kinetics of human fetal and human adult skeletal muscle. The Journal of Physiology. **591,** 3049-3061

12. Ecob-Prince, M., Hill, M., and Brown, W. (1989) Immunocytochemical demonstration of myosin heavy chain expression in human muscle. Journal of the Neurological Sciences. **91,** 71-78

13. Racca, A.W., Beck, A.E., McMillin, M.J., Korte, F.S., Bamshad, M.J., and Regnier, M. (2015) The embryonic myosin R672C mutation that underlies Freeman-Sheldon syndrome impairs cross-bridge detachment and cycling in adult skeletal muscle. Human Molecular Genetics.

14. Beck, A.E., McMillin, M.J., Gildersleeve, H.I.S., Shively, K.M.B., Tang, A., and Bamshad, M.J. (2014) Genotype-phenotype relationships in Freeman-Sheldon syndrome. American Journal of Medical Genetics Part A. **164,** 2808-2813

15. Tajsharghi, H., Kimber, E., Kroksmark, A.K., Jerre, R., Tulinius, M., and Oldfors, A. (2008) Embryonic Myosin Heavy-Chain Mutations Cause Distal Arthrogyposis and Developmental Myosin Myopathy That Persists Postnatally. Archives of Neurology. **65,** 1083-1090

16. Toydemir, R.M., Rutherford, A., Whitby, F.G., Jorde, L.B., Carey, J.C., and Bamshad, M. (2006) Mutations in embryonic myosin heavy chain (MYH3) cause Freeman-sheldon syndrome and Sheldon-Hall syndrome. Nature Genetics. **38,** 561-565

17. Tajsharghi, H., Kimber, E., Kroksmark, A.K., Jerre, R., Tulinius, M., and Oldfors, A. (2008) Embryonic Myosin Heavy-CHain Mutations Cause Distal Arthogryposis and Developmental Myosin Myopathy That Persists Postnatally. Archives of Neurology. **65,** 1083-1090

18. Ontell, M.P., Sopper, M.M., Lyons, G., Buckingham, M., and Ontell, M. (1993) Modulation of contractile protein gene expression in fetal murine crural muscles: Emergence of muscle diversity. Developmental Dynamics. **198,** 203-213

19. Preller, M., and Holmes, K.C. (2013) The myosin start-of-power stroke state and how actin binding drives the power stroke. Cytoskeleton. **70,** 651-660

20. Sweeney, H.L., and Houdusse, A. (2010) Structural and functional insights into the myosin motor mechanism. Annual Reviews of Biophysics. **39,** 539-557

21. Resnicow, D.I., Deacon, J.C., Warrick, H.M., Spudich, J.A., and Leinwand, L.A. (2010) Functional diversity among a family of human skeletal muscle myosin motors. Proceedings of the National Academy of Sciences of the United States of America. **107,** 1053-1058

22. Wang, Q., Moncman, C.L., and Winkelmann, D.A. (2003) **Mutations in the motor domain modulate myosin activity and myofibril organization**
 . Journal of Cell Science. **116,** 4227-4238

23. Bloemink, M.J., Deacon, J.C., Langer, S., Vera, C., Combs, A., Leinwand, L.A., and Geeves, M.A. (2014) The Hypertrophic Cardiomyopathy Myosin Mutation R453C alters ATP-binding and hydrolysis of human cardiac β-myosin . The Journal of Biological Chemistry. **289,** 5158-5167

24. Sommese, R.F., Sung, J., Nag, S., Sutton, S., Deacon, J.C., Choe, E., Leinwand, L.A., Ruppel, K., and Spudich, J.A. (2013) Molecular consequences of the R453C hypertrophic cardiomyopathy mutation on human ß-cardiac myosin motor function. Proceedings of the National Academy of Sciences. **110,** 12607-12612

25. Nag, S., Sommese, R.F., Ujfalusi, Z., Combs, A., Langer, S., Sutton, S., Leinwand, L.A., Geeves, M.A., Ruppel, K., and Spudich, J.A. (2015) Contractility parameters of human ß-cardiac myosin with the hypertrophic cardiomyopathy mutation R403Q show loss of motor function. Science Advances. **1,**

26. Bottinelli, R., and Reggiani, C. (2000) Human skeletal muscle fibres: molecular and functional diversity. Progress in Biophysics & Molecular Biology. **73,** 195-262

27. Furch, M., Geeves, M.A., and Manstein, D.J. (1998) Modulation of actin affinity and actomyosin adenosine triphosphatase by charge changes in the myosin motor domain. Biochemistry. **37,** 6317-6326

28. Bagshaw, C.R., and Trentham, D.R. (1973) The Reversibility of Adenosine Triphosphate Cleavage by Myosin. Biochemical Journal. **133,** 323-328

29. Kurzawa, S.E., and Geeves, M.A. (1996) A novel stopped-flow method for measuring the affinity of actin for myosin head freagment using microgram quantities of protein. Journal of Muscle Research and Cell Motility. **17,** 669-676

30. Biasini, M., Bienert, S., Waterhouse, A., Arnold, K., Struder, G., Schmidt, T., Kiefer, F., Cassarino, T.G., Bertoni, M., Bordoli, L., and Schwede, T. (2014) SWISS-MODEL: modelling protein tertiary and quaternary structure using evolutionary information. Nucleic Acids Research. **42,** 252-258

31. Arnold, K., Bordoli, L., Kopp, J., and Schwede, T. (2006) The SWISS-MODEL Workspace: A web-based environment for protein structure homology modelling. Bioinformatics. **22,** 195-201

32. Guex, N., Peitsch, M.C., and Schwede, T. (2009) Automated comparative protein structure modeling with SWISS-MODEL and Swiss-PdbViewer: A historical perspective. Electrophoresis. **30,** 162-173

33. Kiefer, F., Arnold, K., Künzil, M., Bordoli, L., and Schwede, T. (2009) The SWISS-MODEL Repository and associated resources. Nucleic Acids Research. **37,** 387-382

34. Bloemink, M.J., Adamek, N., Reggiani, C., and Geeves, M.A. (2007) Kinetic analysis of the slow skeletal myosin MHC-1 isoform from Bovine masseter muscle. Journal of Molecular Biology. **373,** 1184-1197

35. Cooke, R., and Pate, E. (1985) The effects of ADP and Phosphate on the contraction of muscle fibers. Biophysical Journal. **48,** 789-798

36. Siemankowski, R.F., Wiseman, M.O., and White, H.D. (1985) ADP dissociation from actomyosin subfragment 1 is sufficiently slow to limit the unloaded shortening velocity in vertebrate muscle. Proceedings of the National Academy of Sciences of the United States of America. **82,** 658-662

37. Deacon, J.C., Bloemink, M.J., Rezavandi, H., Geeves, M.A., and Leinwand, L.A. (2012) Erratum to: Identification of functional differences between recombinant human α and β cardiac myosin motors. Cellular and Molecular Life Sciences. **69,** 4239-4255

38. Bloemink, M.J., and Geeves, M.A. (2011) Shaking the myosin family tree: Biochemical kinetics defines four types of myosin motor. Seminars in Cell & Developmental Biology. **22,** 961-967

39. Geeves, M.A., and Holmes, K.C. (1999) Structural mechanism of muscle contraction. Annual Review of Biochemistry. **68,** 687-728

40. Málnási-Csizmadia, A., Pearson, D.S., Kovács, M., Woolley, R.J., Geeves, M.A., and Bagshaw, C.R. (2001) **Kinetic Resolution of a Conformational Transition and the ATP Hydrolysis Step Using Relaxation Methods with a Dictyostelium Myosin II Mutant Containing a Single Tryptophan Residue**. Biochemistry. **40,** 12727-12737

41. Bloemink, M.J., Deacon, J.C., Resnicow, D.I., Leinwand, L.A., and Geeves, M.A. (2013) The Superfast Human Extraocular Myosin Is Kinetically Distinct from the Fast Skeletal IIa, IIb, and IId Isoforms. The Journal of Biological Chemistry. **288,** 27469-27479

42. Wheeler, S.E., and Bloom, W.G. (2014) **Toward a More Complete Understanding of Noncovalent Interactions Involving Aromatic Rings**
 . The Journal of Pyhsical Chemistry A. **118,** 6133-6147

43. Dougherty, D.A. (1996) Cation-π Interaction in Chemistry and Biology: A New View of Benzene, Phe, Tyr, and Trp. Science. **271,** 163-168

44. Fischer, S., Windschügel, B., Horak, D., Holmes, K.C., and Smith, J.C. (2005) Structural mechanism of the recovery stroke in the Myosin molecular motor. Proceedings of the National Academy of Sciences. **102,** 6873-6878

45. Mijailovich, S.M., Stojanovic, B., Djordje, N., and Geeves, M.A. (2015) Activation and releaxation kinetics in skeletal and cardiac muscles. Biophysical Journal. **108,** 337a-338a

46. Mijailovich, S.M., Djordje, N., Svicevic, M., Stojanovic, B., and Geeves, M.A. (2015) Modelling the calcium dependent actin-myosin ATP-ase cycle in solution. Biophysical Journal. **108,** 594a

Table 1: Transient kinetic parameters measured for wild type beta and embryonic, R672H, R672C, and T178I myosin S1 mutations. The values represent the mean ± SEM based on a minimum of three different protein preparations. All measurements were performed at 20 °C in 25 mM KCl, 20 mM MOPS, 5 mM $MgCl_2$, 1 mM DTT (pH 7) unless stated otherwise. Shaded boxes show the values that have changed significantly.

Rate Constant	Wild Type β [a]	Wild type Emb	Emb R672H	Emb R672C	Emb T178I
ATP binding to S1					
K_1k_{+2} (μM^{-1} s^{-1})	5.8 ± 0.4 [b]	12.5 ± 1.9	0.4 ± 0.04 [d]	1.1 ± 0.07 [d]	2.3 ± 0.1 [c]
$1/K_1$ (μM)	15.9 ± 1.4	10.9 ± 2.0	34.4 ± 5.0 [b]	23.6 ± 2.6 [b]	7.7 ± 0.6
k_{+2} or $k_{+3} + k_{-3}$ (s^{-1})	91.2 ± 1.8 [d]	130 ± 3.4	14.3 ± 0.5 [d]	25.4 ± 1.3 [d]	17.7 ± 0.6 [d]
ADP binding to S1					
K_5 (μM)	0.53 ± 0.07 [b]	0.15 ± 0.018	-	0.2 ± 0.04	-
k_{+5} (s^{-1})	0.63 ± 0.03 [b]	0.89 ± 0.07	-	-	-
ATP binding to acto-S1					
$K'_1k'_{+2}$ (μM^{-1} s^{-1})	4.4 ± 0.2 [b]	9.4 ± 1.0	4.5 ± 0.3 [c]	2.2 ± 0.5 [d]	3.3 ± 0.2 [d]
$1/K'_1$ (μM)	327.9 ± 53.3 [b]	84.3 ± 9.7	92.3 ± 9	120 ± 19.3	317.7 ± 41.1 [c]
k'_{+2} (s^{-1})	1543 ± 100 [b]	777.7 ± 16.8	413 ± 32.2 [d]	261 ± 8.4 [d]	1033.2 ± 60.2 [b]
K_α	4.1 ± 1.4	-	4.4 ± 0.8	-	6.9 ± 1
$k_{+\alpha}$ (s^{-1})	153.4 ± 10.6	-	31.5 ± 2.5	-	66.1 ± 9.1
ADP binding to acto-S1					
K'_5 (μM)	6.1 ± 0.3 [b]	14.3 ± 1.9	4.8 ± 0.5 [c]	18.1 ± 1.7	12.4 ± 2.2
k'_{+5} (s^{-1})	58.7 ± 1.7 [d]	22.0 ± 1.8	7.4 ± 0.2 [d]	18.6 ± 1.1	25.7 ± 0.5
S1 affinity for actin					
K_A (nM)	10 ± 1.8 [b]	2.1 ± 0.2	40.2 ± 2.1 [d]	7.2 ± 1.2 [b]	4.8 ± 0.2 [d]
K_{DA} (nM)	109.3 ± 24.1 [d]	526 ± 60.3	366.7 ± 31	331.3 ± 68.6	123.5 ± 15.1 [d]
K_{DA}/K_A	10.9	250	9	46	25.7
K'_5/K_5	11.5	95	-	90.5	-
ATPase *					
V_{max} (s^{-1})	6.0 ± 0.5	7.0 ± 0.15	1.3 ± 0.05 [d]	3.5 ± 0.05 [d]	0.2 ± 0.008 [d]
K_M (μM)	40 ± 6	38.5 ± 2.4	3.7 ± 0.7 [c]	4.6 ± 0.3 [d]	0.67 ± 0.16 [d]
V_{max}/K_M (s^{-1} μM^{-1})	0.15	0.18	0.35	0.76	0.30

*KCl concentration 0 mM

[a] Nag et al in same ionic strength as this experiment obtained from C2C12 cells.

[b] $p < 0.05$ determined by Student's t test as compared to wild type embryonic-S1.

[c] $p < 0.01$ determined by Student's t test as compared to wild type embryonic-S1.

[d] $p < 0.001$ determined by Student's t test as compared to wild type embryonic-S1.

Table 2a. Full list of interactions between R672 in WT MyHC-emb and the two R672 mutants. There are interactions between R672, on β3, and C123 and T125, on β2 of the central β sheet in most conformations. The exception being the contact to C123 in the near rigor, ADP-bound state (PDB 1S5G). These interactions are predicted to be conserved in the R672C and R672H mutations. A π-cation bond that exists between R672 and F122 (β2) in the rigor state (2OS8) and is lost in both mutations but a novelπ-π bond is formed between R672H and F122 in the rigor state (2OS8). The hydrogen bond between R672 and L176 (β1) is also lost in both mutations in the rigor state. T178 (on β4) hydrogen bonds to R672 in each structure; however, this interaction is lost in the post-rigor (1SR6) and the detached (1KK8) states for R672H and are lost completely for R672C. A second significant loss of interaction is the π-cation bond between R672 and F490 on the relay helix, which is non-existent in either mutation. A π-cation bond to F670 is lost for both mutations in the detached state, however a π-π bond is formed in the pre-power state (1QVI). A hydrogen bond between V671 is present in WT MyHC-emb in the rigor and post rigor states (1OS8, 2OTG, and 1SR6) but lost in both mutations. The hydrogen bond between N697 on the SH1-SH2 domain is conserved in all three models in the rear rigor ADP-bound state (1S5G). However this is lost in R672H in the detached state (1KK8) and in R672C, in the post-rigor state (1SR6). Interestingly, this interaction is formed in both mutants in the rigor (1KK8) and post-rigor (2OTG) states.

R672 interactions	PDB		2OTG	2OS8	1SR6	1QVI	1KK8	1S5G
Residue (Scallop/Homology)	Location	Interaction	post-rigor (ADP)	rigor	post-rigor	pre-power	detached	near rigor ADP-
F119/F122	β2	π-cation/π-π bond						
C120/C123	β2	H-bond (main chain)						
A122/T125	β2	H-bond (main chain)						
L173/L176	β4	H-bond (side chain)						
T175/T178	β4	H-bond (side chain)						
F488/F490	Relay helix	π-cation bond						
F667/F670	β3	π-cation/π-π bond						
V668/V671	β3	H-bond (side chain)						
N694/N697	SH1-SH2	H-bond (side chain)						

	Interaction present in wt
	Interaction present in R672H
	Interaction present in R672C
	No interaction

Table 2b: Full list of interactions between T178 in WT MyHC-emb and T178I. The only change in the T178I mutation is the complete loss of the hydrogen bond between T178 and R672. The other two interactions between V671 and C673 (both on β3) are both intact (except V671 in the post-rigor state – 2OTG, which is not present in WT MyHC-emb or T178I).

T178I	PDB		2OTG	2OS8	1SR6	1QVI	1KK8	1S5G
Residue (Scallop/Homology)	Location	Interaction	post-rigor (ADP)	rigor	post-rigor	pre-power	detached	near rigor ADP-bound
V668/V671	β3	H-bond (main chain)						
R669/R672	β3	H-bond (side chain)						
C670/C673	β3	H-bond (main chain)						

	Interaction present in wt
	Interaction present in T178I
	No interaction

Figure 1: Homology model of embryonic myosin S1. This ribbon structure is based on the scallop structure in the pre-power stroke conformation (PDB code: 1QVI). (A) The myosin heavy chain is shown in grey, the SH1-SH2 helices are shown in orange; the relay helix in yellow, the P-loop in purple, and the 7 stranded β sheet in red. Arginine 672 (R672) and Threonine 178 (T178) residues are shown in green and blue space filling mode respectively. Both of these residues are highly conserved across species and myosin-II isoforms including the scallop myosin and human MyHC-emb. Both residues are in the centre of the S1 domain located in the upper 50K domain near the ATP binding cleft. (B) Blow up of the region around R672 (located on the 3rd β strand) and T178 on the 4th β strand of the 7 stranded β-sheet that runs through the S1 domain. T178 is also at the base of the P-loop (GESGAG residue no.) which is involved in ATP binding. The green dotted lines represent hydrogen bonds which can be seen between T178 and R672, while the solid orange line indicates a π-cation bond that can be seen between R672 and F490. The interactions of R672 and T178 are summarised in Table 2. Residues not labelled are those found to interact with either R672, T178 or both and are summarised in Tables 2A/B.

Figure 2: SDS-PAGE gel of purified wild type embryonic S1. The myosin S1 co-purifies with a small amount of endogenous mouse full length myosin (<5% by weight) and the four mouse light chains; three major bands MLC2F (regulatory), MLC1F, and MLC1A (both essential) and a minor band of MLC3F. The three major bands have been identified in embryonic S1 (Bottinelli & Reggiani, 1996) suggesting that the fourth (?) light chain (MLC3F) is binding to the endogenous myosin.

Figure 3: ATP induced dissociation of embryonic S1 from pyrene labelled actin. (A) Traces of 50 nM WT emb-S1, and the three mutants pre-incubated with equimolar pyrene-labelled actin then rapidly mixed with 10 μM ATP. Each trace has been normalised and offset by the previous one by 0.2% fluorescence. At low [ATP] WT MyHC-emb, R672C, and T178I were best described by a single exponential fit resulting in a k_{obs} = 70 s^{-1} (amp = 27%), 12 s^{-1} (amp = 46%), 24 s^{-1} (amp = 45%) for WT MyHC-emb, R672C, and T178I respectively. At high [ATP] the T178I mutation was best described by a double exponential, while R672H was best described by a double exponential at all [ATP] resulting in a fast and slow phase giving k_{obs} = 36 s^{-1} (amp = 32%) and k_{obs} = 4.4 s^{-1} (amp = 3.8%) respectively. (B) The dependence of k_{obs} on [ATP] yielded $K'_1k'_{+2}$ = 8.5 μM^{-1} s^{-1}, 5.2 μM^{-1} s^{-1}, 1.8 μM^{-1} s^{-1}, and 3.1 μM^{-1} s^{-1} for WT MyHC-emb (black filled squares), R672H (red filled circles), R672C (green filled triangles), and T178I (blue filled diamonds). The maximum rate yielded a k'_{+2} = 806 s^{-1} for WT MyHC-emb , 439 s^{-1} and 36 s^{-1} for the R672H fast and slow (red open circles) phases respectively, 262 s^{-1} for R672C, and 1007 s^{-1} and 49 s^{-1} for the T178I fast and slow (blue open diamonds) phases respectively. Values given here are that of a single assay.

Figure 4: ADP affinity for pyrene-labelled actin.S1. (A) Fluorescent traces of 50 nM pyrene-labelled actin pre-incubated with 50 nM WT MyHC-emb and increasing [ADP] (0-400 μM) rapidly mixed with 10 μM ATP. As the [ADP] increased the k_{obs} decreased from 72 s^{-1} to 3 s^{-1}. (B) The dependence of k_{obs} on [ADP] for WT MyHC-emb (squares) and T178I (circles) resulting in a K'_5 = 16 ± 1.5 μM and 17 ± 4 μM respectively. (C) Traces of 50 nM pyrene-actin pre-incubated with 50 nM R672H S1 and increasing [ADP] (0-40 μM) rapidly mixed with 30 μM ATP. Since there was a consistent slow phase even at low [ATP] the rates stayed constant while the amplitude of the fast phase decreased from 26% to 6%, the slow phase amplitude increased from 3.5% to 21%. This behaviour was also seen in the R672C mutation. (D) The dependence of fluorescence amplitude of [ADP] for R672H results in a K'_5 = 2.6 ± 1.1 μM for the fast phase and K'_5 = 5 ± 1.3 μM for the slow phase.

Figure 5: Embryonic S1 affinity for actin in the absence and presence of ADP. (A) Traces of increasing concentrations (0 μM to 120 nM) of WT MyHC-emb pre-incubated with 30 nM pyrene-labelled actin then rapidly mixed with 10 μM ATP. Over a concentration series the fluorescence amplitude increased with [S1]. (B) The dependence of amplitude on [S1] can be described by a quadratic function (Eq. 6) giving a K_A value of 2.5 nM for WT MyHC-emb (filled squares), 43 nM for R672H (open squares), 6.1 nM for R672C (filled circles), and 5.2 nM for T178I (open circles). (C) Repeating the same experiment but this time incubating the acto.S1 with saturating [ADP]. Plotting the amplitude against the [S1] again gives a quadratic dependence which in turn gives a K_{DA} value of 706 nM for WT MyHC-emb (filled squares), 306 nM for R672H (open squares), 386 nM for R672C (filled circles),

and 71 nM for T178I (open circles). Concentrations of S1 are before mixing.Add panel D here with ADP release exp data

Figure 6: Nucleotide binding to embryonic S1. (A) Tryptophan fluorescence changes observed on rapidly mixing 50 µM ATP with 100 nM WT MyHC-emb and for the three mutants S1s. All four were best described with a single exponential fit yielding k_{obs} = 102 s^{-1} (amplitude = 6.6%), 7.3 s^{-1} (amplitude = 1.6%), 12 s^{-1} (amplitude = 3.5%), 18 s^{-1} (amplitude = 1.4%) for WT MyHC-emb, R672H, R672C, and T178I respectively. The single exponential fits are shown with solid black lines. (B) The hyperbolic dependence of k_{obs} on [ATP] yielded K_1k_{+2} = 8.8 μM^{-1} s^{-1}, 0.3 μM^{-1} s^{-1}, 0.95 μM^{-1} s^{-1}, and 2.1 μM^{-1} s^{-1} for WT MyHC-emb (filled squares), R672H (open squares), R672C (filled circles), and T178I (open circles) respectively. The maximum rate gives a value of k_{max} = 134 s^{-1} for WT MyHC-emb, 15.2 s^{-1} for R672H, 25 s^{-1} for R672C, and 17.8 s^{-1} for T178I. (C) The protein fluorescence observed after mixing 0.1 µM WT MyHC-emb pre-incubated with 50 nM ADP with 50 µM ATP. The data could be best described by a double exponential function with a fast phase (k_{obs} = 92 s^{-1} and amp = 5.9%) and a slow phase (k_{obs} = 1 s^{-1} and amp = 1.3%). (D) The dependence of the amplitudes of the fast and slow phases on [ADP] was hyperbolic resulting in a K_D = 0.13 ± 0.06 µM for the fast phase (filled squares) and K_D = 0.12 ± 0.03 µM for the slow phase (open squares). This measurement was not possible with the R672H or T178I mutations while there was only one phase for the R672C.

Figure 7: ATPase assays of the WT MyHC-emb and the three FSS mutations. (A) The actin activation of the S1 ATPases with best fit Michaelis-Menten curves superimposed on the data points. These fits gave a V_{max} = 7.0 s^{-1} for WT MyHC-emb and a K_M = 38.5 µM (filled squares). The R672H (filled circles) had a V_{max} = 1.3 s^{-1} and a K_M = 3.7 µM, R672C (open squares) a V_{max} = 3.5 s^{-1} and a K_M = 4.6 µM, and T178I (open circles) a V_{max} = 0.2 s^{-1} and a K_M = 0.7 µM. (B) The ATPase assay of the T178I mutant on a log time scale to highlight the T178I fit to a Michaelis-Menten function despite a small activation by actin. Results plotted are from two protein preps with 3-4 technical replicates each time.

Figure 8: Homology model of WT MyHC- emb showing the relay helix, R672 and F122, F490, and F670 in rigor and pre-power stroke. (A) Structure based on scallop structure (PDB code: 2OS8) where the motor domain is in the rigor conformation and the relay helix is straight (Blue). There is a single π-cation bond between R672 and F490 shown in orange. A superimposed second relay helix (in red) is based on scallop structure in the pre-power stroke conformation (PBB code: 1QVI). The relay helix is bent just after F490 and the π-cation interaction between R672 and F490 remains. (B) R672 (blue), F489 (orange), F490 (green), and F670 (red) are shown with the relay helix to illustrate the phenylalanine residues acting as pivot point for the relay helix bend. R672's proximity and interactions with the F490 possibly anchor the helix allowing it to bend.

Figure 9: Percentage changes in the rate and equilibrium constants of WT MyHC-emb compared to WT MyHC-β (A & B) and the three FSS mutations compared to WT MyHC-emb (C & D). (A & C) Equilibrium constants are defined in M units; a positive percentage means an increase in affinity while a negative indicates a weakening of affinity. (B & D) The rate constants are define in units of s-1 or M-1s-1 and a positive percentage indicates a faster rate constant while a negative percentage, a slower rate constant. ns = not significant, * = $p<0.05$, ** = $p<0.01$, *** = $p<0.001$.

Scheme 1: Seven step scheme of ATP binding to myosin

Scheme 2: ATP or ADP binding to actomyosin leading to the dissociation of myosin from actin.

Figure 1

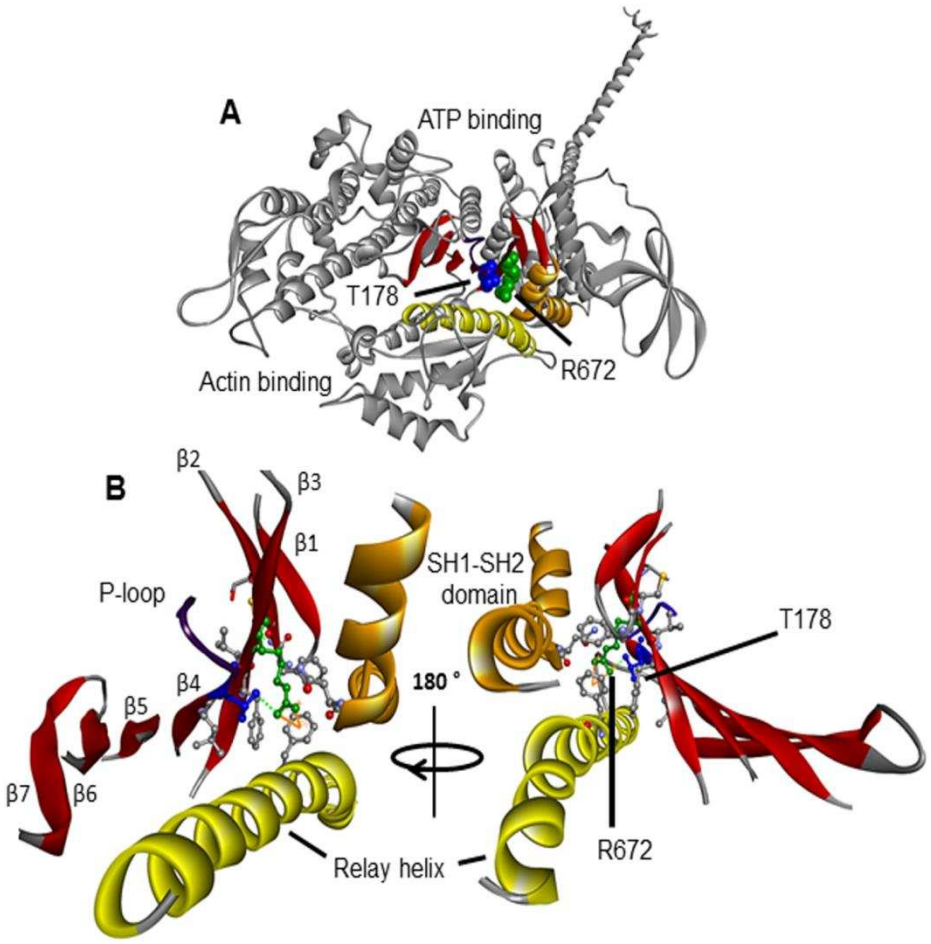
A
ATP binding
T178
R672
Actin binding
B
β2
β3
β1
P-loop
SH1-SH2
domain
T178
β4
180 °
β5
β7
β6
R672
Relay helix

Figure 2

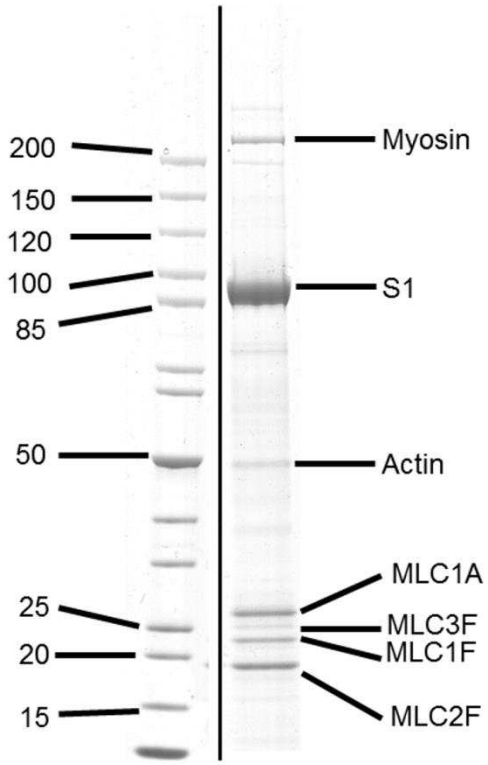
200
150
120
100
85
50
25
20
15
Myosin
S1
Actin
MLC1A
MLC3F
MLC1F
MLC2F

Figure 3

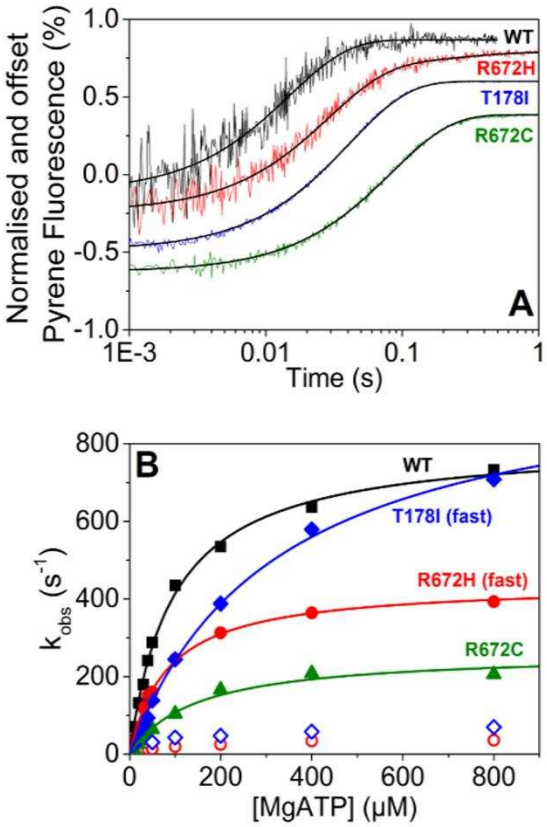
Normalised and offset
Pyrene Fluorescence (%)
1.0
0.5
0.0
-0.5
-1.0
1E-3
0.01
0.1
1
Time (s)
WT
R672H
T178I
R672C
A
800
600
400
200
0
0
200
400
600
800
[MgATP] (μM)
k_{obs} (s^{-1})
B
WT
T178I (fast)
R672H (fast)
R672C

Figure 4

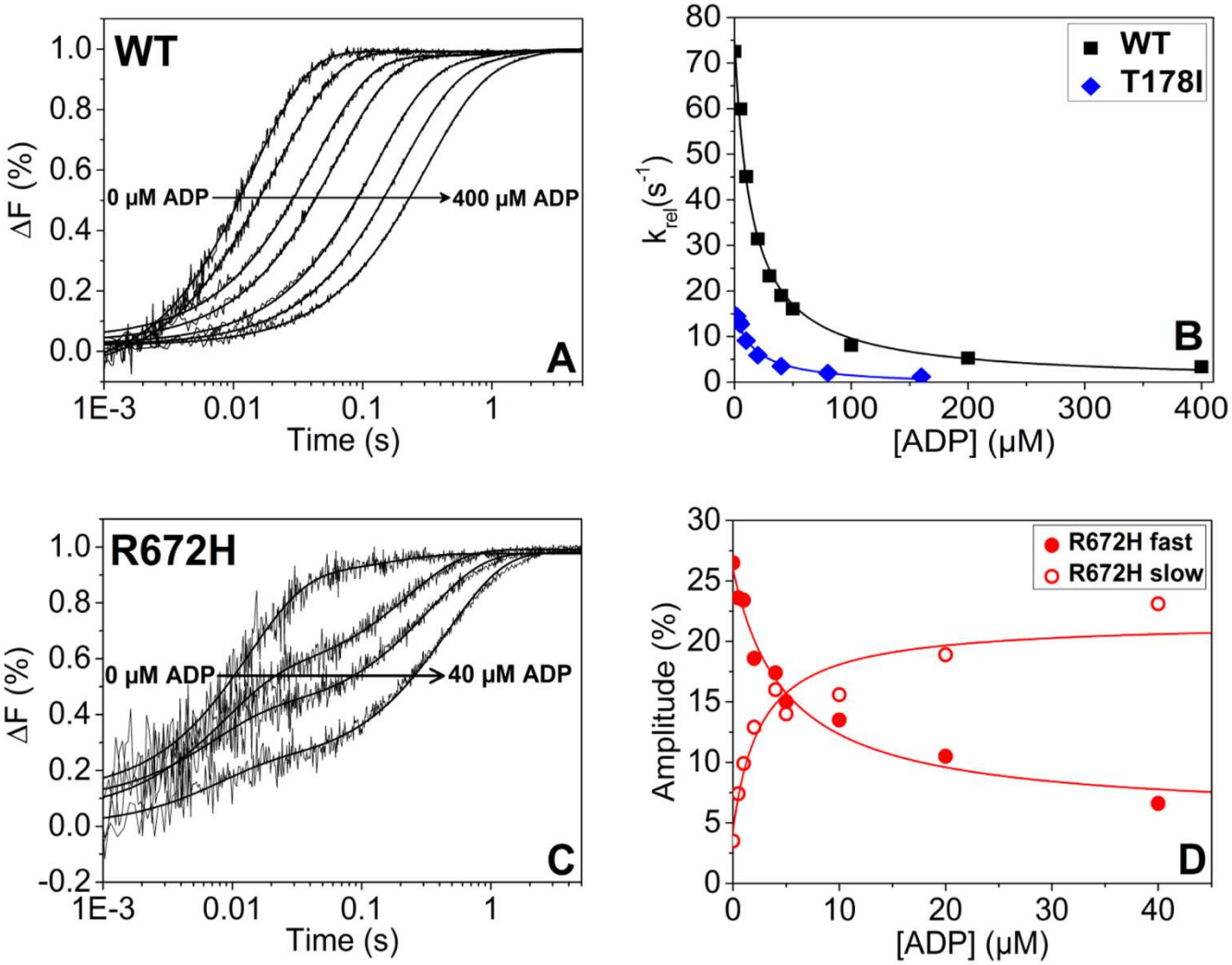
WT
0 µM ADP
400 µM ADP
ΔF (%)
Time (s)
A
WT
T178I
k_{rel} (s^{-1})
[ADP] (µM)
B
R672H
0 µM ADP
40 µM ADP
ΔF (%)
Time (s)
C
R672H fast
R672H slow
Amplitude (%)
[ADP] (µM)
D

Figure 5

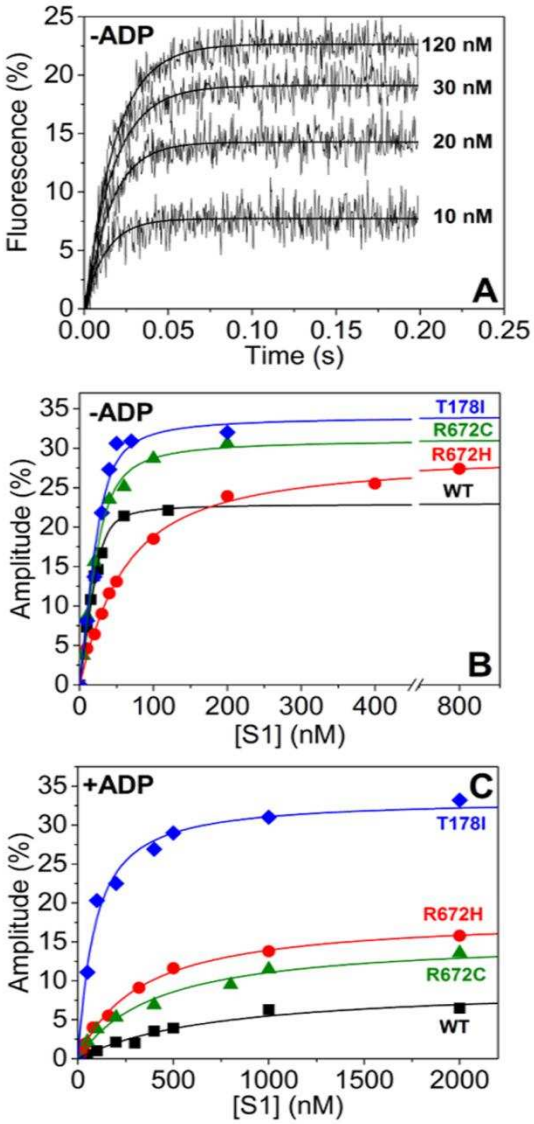
-ADP
120 nM
30 nM
20 nM
10 nM
A
Fluorescence (%)
Time (s)
-ADP
T178I
R672C
R672H
WT
B
Amplitude (%)
[S1] (nM)
+ADP
C
T178I
R672H
R672C
WT
Amplitude (%)
[S1] (nM)

Figure 6

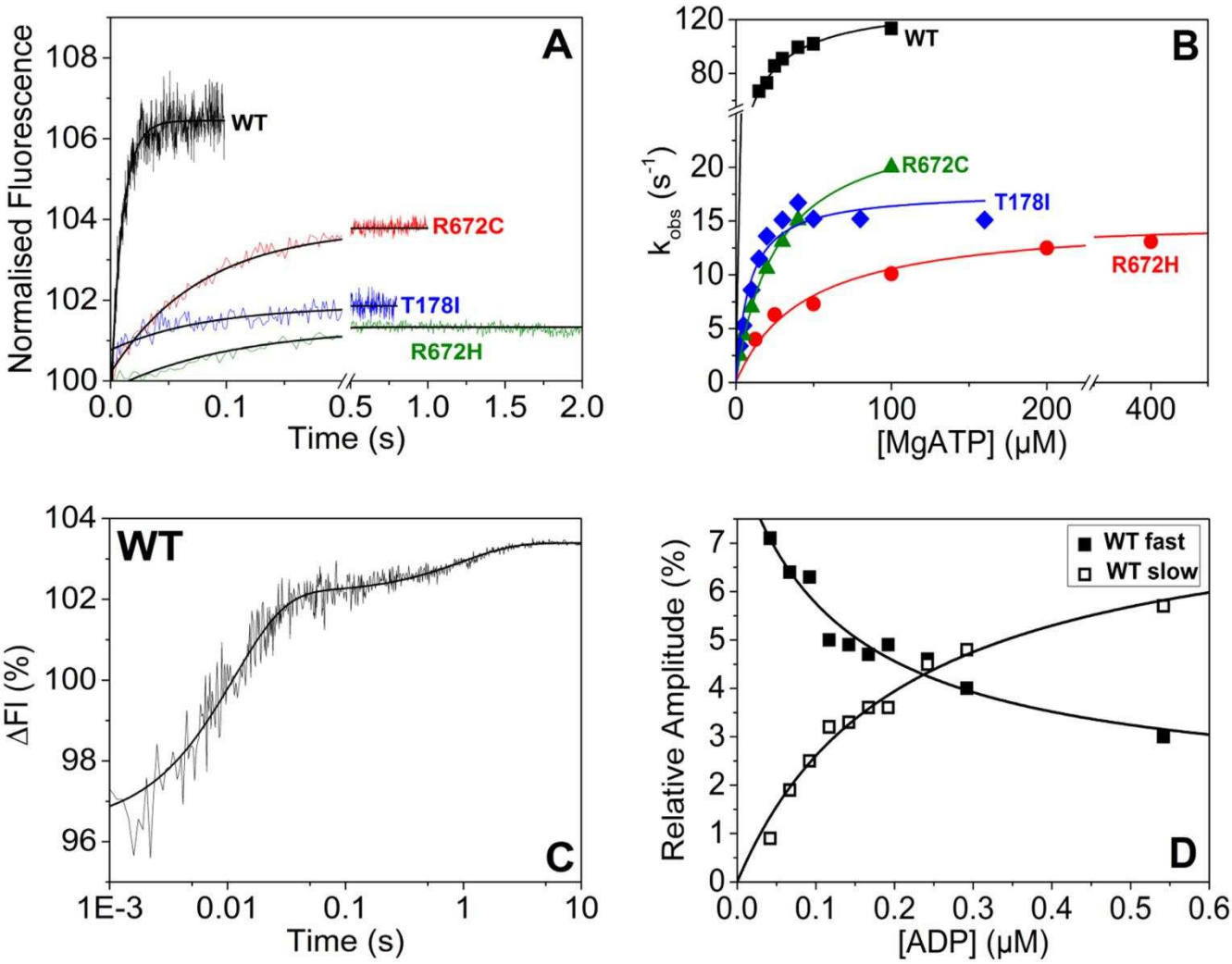
A
Normalised Fluorescence
Time (s)
WT
R672C
T178I
R672H
B
k_{obs} (s^{-1})
[MgATP] (μM)
WT
R672C
T178I
R672H
C
WT
ΔFl (%)
Time (s)
D
Relative Amplitude (%)
[ADP] (μM)
WT fast
WT slow

Figure 7

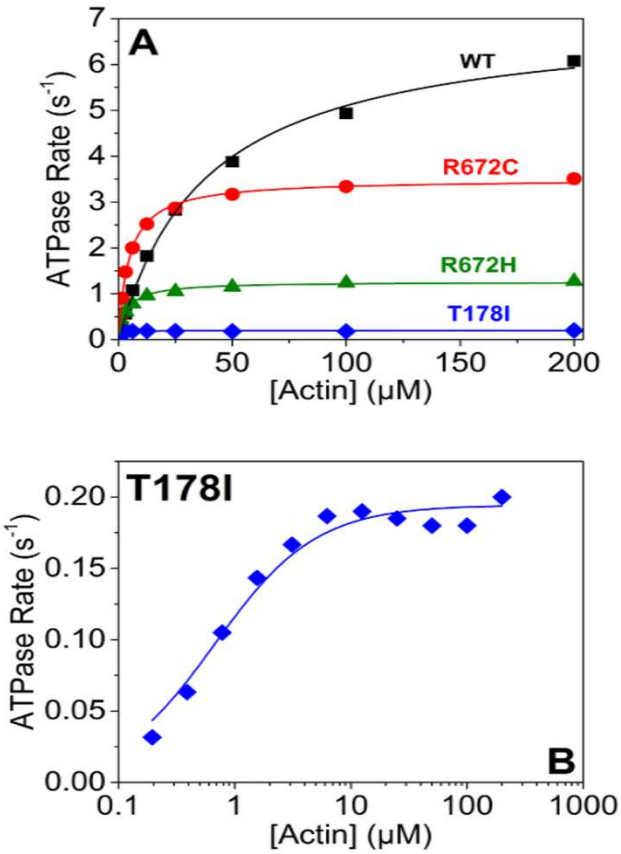
A
WT
R672C
R672H
T178I
ATPase Rate (s-1)
[Actin] (μM)
0
1
2
3
4
5
6
7
0
50
100
150
200
T178I
B
ATPase Rate (s-1)
[Actin] (μM)
0.00
0.05
0.10
0.15
0.20
0.1
1
10
100
1000

Figure 8

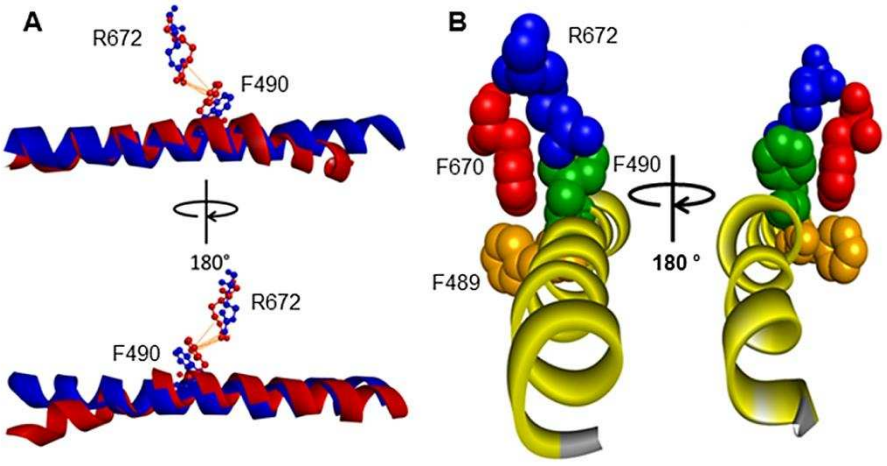

Figure 9

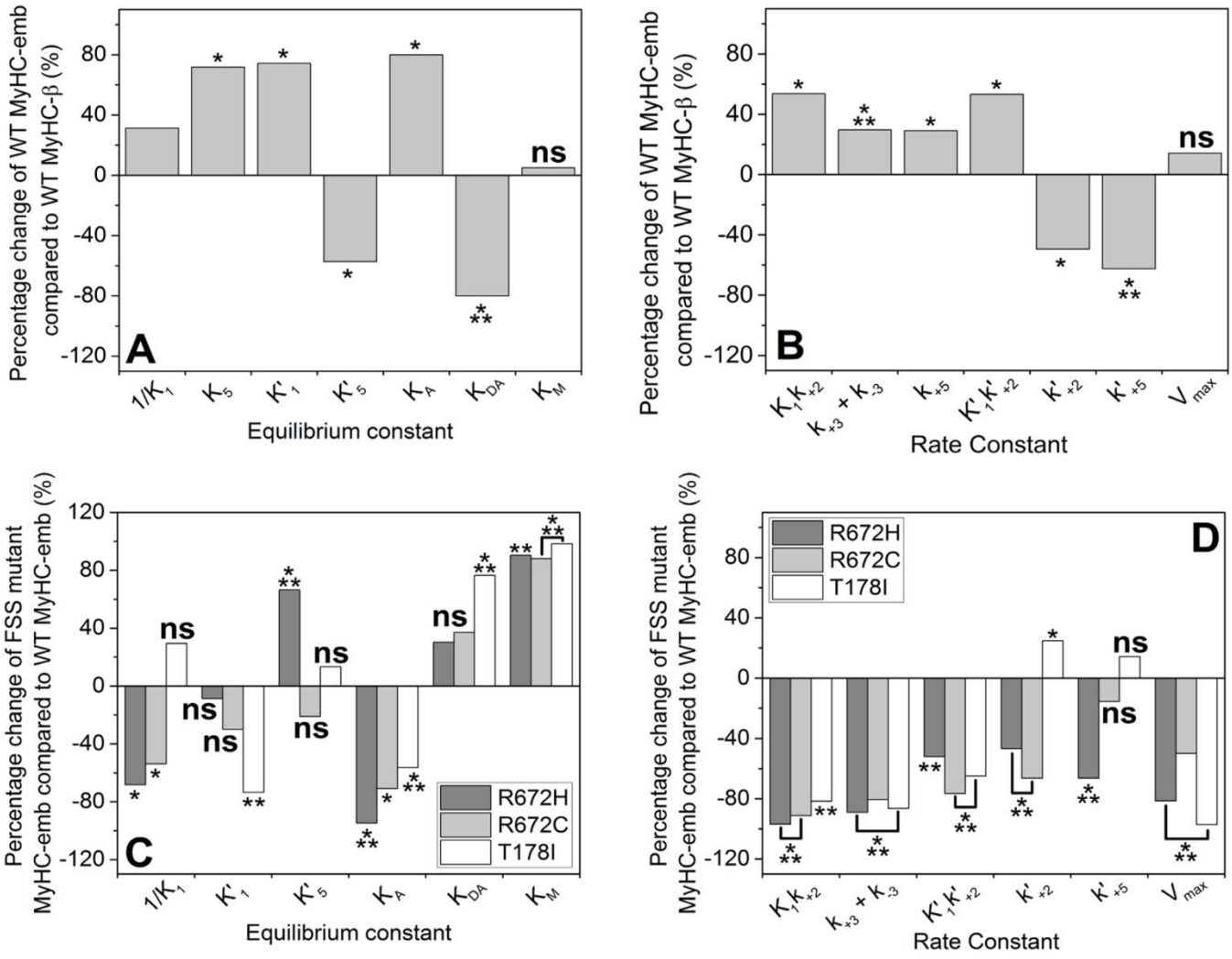
Percentage change of WT MyHC-emb compared to WT MyHC-β (%)
A
ns
Equilibrium constant
B
Rate Constant
Percentage change of FSS mutant MyHC-emb compared to WT MyHC-emb (%)
C
R672H
R672C
T178I
Equilibrium constant
D
R672H
R672C
T178I
Rate Constant

Scheme 1

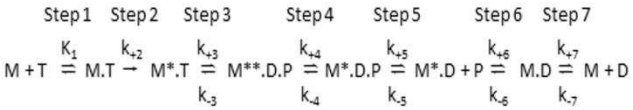

Scheme 2